Environmental Science Nano

Interaction of Beta-Lactoglobulin and Bovine Serum Albumin with Iron Oxide (α-Fe2O3) Nanoparticles in the Presence and Absence of Pre-Adsorbed Phosphate

Journal:	*Environmental Science: Nano*
Manuscript ID	EN-ART-04-2021-000388.R2
Article Type:	Paper

Interaction of Beta-Lactoglobulin and Bovine Serum Albumin with Iron Oxide (α-Fe_2O_3) Nanoparticles in the Presence and Absence of Pre-Adsorbed Phosphate

Irem B. Ustunol,[a] Elizabeth K. Coward,[b] Eleanor Quirk,[a] and Vicki H. Grassian[a,b,c,*]

[a] Department of Nanoengineering, [b] Department of Chemistry and Biochemistry, and
[c] Scripps Institution of Oceanography, University of California, San Diego, La Jolla, CA, 92093

Conformational changes of proteins during adsorption to oxide nanoparticle surfaces drive both protein function and nanoparticle reactivity in the environment. However, changes in protein structure at the oxide nanoparticle surface are currently poorly-characterized under different environmentally-relevant conditions where multiple species exist. Using attenuated total reflectance-Fourier transform infrared (ATR-FTIR) spectroscopy, this work investigates conformation changes of two proteins, distinct in size and flexibility, adsorbed on α-Fe_2O_3 nanoparticle surfaces in the presence and absence of pre-adsorbed phosphate. These findings provide insight into the role of adsorbed oxyanions on protein coverage, corona formation, and oxide nanoparticle-bio interactions in environmental systems.

Interaction of Beta-Lactoglobulin and Bovine Serum Albumin with Iron Oxide (α-Fe_2O_3) Nanoparticles in the Presence and Absence of Pre-Adsorbed Phosphate

Irem B. Ustunol,[a] Elizabeth K. Coward,[b] Eleanor Quirk,[a] and Vicki H. Grassian[b*]

[a] Department of Nanoengineering, [b] Department of Chemistry and Biochemistry, University of California, San Diego, La Jolla, CA, 92093

Abstract. Protein adsorption onto mineral nanoparticle surfaces is critical to the function and fate of biological compounds in environmental and industrial systems. However, adsorption kinetics, coverage, and conformation of biological macromolecules are poorly understood, particularly in the presence of ubiquitous oxyanions. In this study, the adsorption of two proteins, beta-lactoglobulin (β-LG) and bovine serum albumin (BSA), onto hematite (α-Fe_2O_3) nanoparticles was investigated in the presence and absence of pre-adsorbed phosphate. Using solution and temporal solid-phase attenuated total reflectance-Fourier transform infrared (ATR-FTIR) spectroscopy, our results show dynamic changes in the secondary structures of both proteins when adsorbed onto nanoscale α-Fe_2O_3 surfaces, compared to their unbound conformations. However, these differences were attenuated in the presence of adsorbed phosphate. Adsorbed phosphate significantly reduced the protein surface coverage on iron oxide nanoparticle surfaces, and impacted protein adsorption kinetics. The latter was observed to be protein-specific, with β-LG exhibiting a higher adsorption rate and sigmoidal kinetics compared to slower, more Langmuir-type kinetics of BSA adsorption. Our results reveal the importance of phosphate on protein-mineral adsorption kinetics and conformation, a critical driver of protein function, in complex environmental systems.

Keywords: Protein adsorption, iron oxide nanoparticles, nano-bio interactions, ATR-FTIR, phosphate.

[*] Corresponding author at University of California, San Diego, La Jolla, CA, 92093, USA. *Tel:* +1 858-534-2499, *E-mail address:* vhgrassian@ucsd.edu. ORCID : 0000-0001-5052-0045 (Vicki H. Grassian), 0000-0003-0370-118X (Irem B. Ustunol), 0000-0001-9959-1266 (Eleanor Quirk), 0000-0002-3279-8788 (Elizabeth K. Coward).

1. Introduction

Nanoscale iron oxides, ubiquitous in soils and sediments,[1–4] are well-known sorbents of natural compounds and contaminants due to their high surface area, thermodynamic stability, and subsequent adsorption capacity.[5,6] As such, iron oxide nanoparticles are commonly used as a sorbent in coatings, cosmetics, catalysis, drug delivery, and environmental remediation applications.[7–9] Molecular adsorption and interactions with nanoparticle (NP) surfaces, and the formation of an adsorbed layer, can alter the physicochemical properties of both NPs and sorbates, and thus their functionality in environmental systems. Hematite (α-Fe_2O_3), the most thermodynamically stable iron oxide mineral, with surface terminations that have elevated free energies of formation and surface enthalpies promoting strong water adsorption and interaction with ions, is ubiquitous in the environment.[10,11] Despite the enhanced reactivity of α-Fe_2O_3, adsorption dynamics and stability, particularly in heterogeneous aqueous matrices, are not fully understood.

Of particular importance are surface interactions of α-Fe_2O_3 with biological macromolecules. Proteins, an essential subset of biological macromolecules, play a vital role in environmental and biological processes.[12] Ubiquitous in environmental systems, they are derived as byproducts of human activities and from secretions or lysis of microorganisms, roots, and fungi.[13,14] All proteins, including enzymes, bind to other molecules to perform their inherent functions and associated protein-mediated processes.[15] These processes are often essential to biochemical reactions fundamental to environmental processes and remediation: proteins attach to viruses or bacteria in cell lysis; the enzyme hexokinase binds glucose and adenosine triphosphate (ATP) to catalyze glycolysis.[14,15] Indeed, microbially-derived proteinaceous compounds are found to be abundant at mineral interfaces. [16,17] Most proteins have a high propensity for adsorption at

solid-liquid interfaces due to their amphiphilic—both hydrophilic and hydrophobic—properties.[18] When proteins encounter nanoparticle interfaces in an aqueous environmental and biological *milieu*, they do not behave like rigid particles.[19] Instead, they can form a dynamic layer on nanoparticle surfaces once adsorbed – a *corona*.[20,21,22] The formation of these coronae can influence mineral aggregation, reactivity, toxicity, and transformation.[23] Moreover, adsorbed proteins can change their secondary conformation, mobility, and enzymatic activity.[24–27] Thus, amino acid and protein interactions at the aqueous-nanomaterial interfaces have been widely investigated using various vibrational spectroscopic and computational methods.[28–32]

Previous studies of protein adsorption onto metal oxide nanoparticles, polymers, and other clay surfaces have demonstrated how perturbations in pH, temperature, protein concentration, and nanomaterial surface chemistry can significantly influence adsorption kinetics, adsorbed protein assembly, and protein secondary structure.[18,29,33–36] The latter is of particular importance, as the structural units of protein (i.e., α-helix, *β*-sheet), which form protein domains, drive protein function.[37] Thus, changes in the secondary structures can contribute to altered protein behavior. Domain changes in protein structure have been widely observed during adsorption to nanoparticles. Bovine serum albumin (BSA) during adsorption to hematite in a pure matrix has been recently examined using two-dimensional correlation spectroscopy (2DCOS) of attenuated total reflectance-Fourier transform infrared (ATR-FTIR) spectra.[24] Their results revealed an increase in α-helix structure frequency during initial surface coverage, followed by α-helical structural loss throughout the final stages of the adsorption process. Changes in BSA unfolding have also been observed during adsorption to montmorillonite, largely as a function of concentration.[29] In contrast, a study of beta-lactoglobulin (*β*-LG) and BSA adsorption onto planar hydrophobic surfaces leveraging molecular dynamics (MD) simulations, quartz crystal

microbalance (QCM), and atomic force microscopy (AFM) suggests a compact monolayer on the solid surfaces.[38]

While our understanding of nanoparticle behavior and protein interactions has advanced in model systems, the experimental design often does not account for the natural complexity of aqueous systems. Environmental and biological aqueous systems consist of naturally occurring assemblies of salts, nutrients, oxyanions, and heterogeneous organic compounds, which may compete, co-adsorb, or aggregate with proteins in solution.[39] As such, the adsorption of a biomolecule on the nanoparticle surface depends on adsorption affinity, diffusion kinetics, and solution chemistry as compounds dynamically compete, co-adsorb, and scaffold on the nanoparticle surface driven by their nano-size and large surface-to-mass ratio.[40–44]

Phosphate, a highly abundant nutrient in aqueous soil and groundwater systems,[45] can impact protein surface adsorption.[26] Inorganic and organic phosphate compounds accumulate in environmental systems, catalyzing harmful algal growth (eutrophication) and the proliferation of aquatic plants, and have been identified as pollutants of concern in groundwater.[46,47] Phosphate provides a pH-stable environment[48] and can itself adsorb onto nanoparticles,[49] occupying active sites on mineral surfaces.[50] However, despite the ubiquitous presence of phosphate in environmental systems, the dynamics of protein adsorption onto iron oxide surfaces in the presence of phosphate are not fully understood.

To probe protein interactions under environmentally- and biologically-relevant conditions, β-LG and BSA were adsorbed to α-Fe_2O_3 nanoparticles in the presence and absence of phosphate at pH 6, just above the isoelectric points for these proteins. These model proteins represent endmembers of protein size, flexibility, and native conformation.[51] β-LG is a small (162 amino acids), rigid protein and is considered to be a model for a 'hard' protein that does not experience

significant structural alterations after adsorption onto surfaces (Table 1).[38] β-LG is a globular protein with predominantly β-sheet structure[51] and one of the major allergens in cow's milk.[52] Because of their relevance to food and dairy processing, there have been several studies on the denaturing conditions (pH and temperature) of β-LG.[53] Additionally, the heat-induced aggregation of β-LG is also used as a model for fibril formation of neurodegenerative disease.[54] In comparison, BSA has a larger size (582 amino acids) and is considered to be a 'soft' protein model, as it undergoes a conformational change upon surface adsorption[26,35]. It also differs from β-LG in that BSA mainly consists of α-helix in aqueous media in its crystal structure.[26,55] BSA is often used as a model protein in many studies due to its high abundance, low cost, and its similarity to human serum albumin (HSA).[26] By comparing the adsorptive behavior of these two model proteins, we can begin to understand the structural and kinetic effects of phosphate pre-adsorption on protein surface interactions, conformation changes, and subsequent behavior in aqueous systems.

Such interactions were investigated using ATR-FTIR spectroscopy, which provides an understanding of real-time biomolecule-surface interactions in a multi-component environment. Solution-phase secondary structural analysis of β-LG and BSA proteins in the amide I region was compared to that of adsorbed proteins, both in the presence and absence of phosphate, using deconvolution analysis to understand the conformational changes upon adsorption. In doing so, this work aims to investigate the dual impacts of protein structure and phosphate pre-adsorption on protein conformation at the α-Fe_2O_3 nanoparticle surface, providing insights into protein interactions at geochemical nanoscale interfaces under increasingly complex conditions.

2. Materials and Experimental Methods

2.1 Materials. α-Fe_2O_3 nanoparticles were purchased from Alfa Aesar, MA. Hematite was chosen due to its presence in diverse environmental systems, from atmospheric dust to many soils and

sediments.[56] Investigations of hematite-contaminant sorption also suggest that these phases are highly reactive, particularly with both ions and organic compounds.[3] The lyophilized proteins of *β*-LG (≥90%) and BSA (≥99.5%) were purchased from Sigma-Aldrich. Characteristics of the proteins used in this study and their crystal structures are shown in Table 1. A phosphate buffer solution of 250 μM $Na_2HPO_4 \cdot H_2O$ (Fisher Scientific, Inc.) used to probe phosphate co-adsorption dynamics was adjusted to pH 6 using hydrochloric acid (HCl) and sodium hydroxide (NaOH) solutions from Fisher Scientific, Inc. All solutions were prepared with Milli-Q water (Millipore, resistance = 18.2 MΩ.cm at 25 °C), and NaCl (Fisher Scientific, Inc.) was used to maintain 10 mM ionic strength through the experiments. All chemicals were used as received without further purification.

Table 1. Protein properties and crystal structures of BSA and *β*-LG. Protein Data Base (PDB) numbers of protein virtual models are 4F5S and 1BEB, respectively.[33,57]

	Bovine Serum Albumin (BSA)	***β*-Lactoglobulin (*β*-LG)**
Protein crystal structure		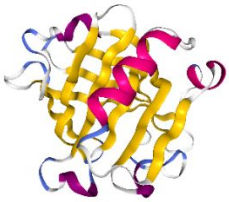
Number of amino acids	582	162
Isoelectric point (pH_{IEP})	4.9	5.1
Conformational rigidity	Soft	Hard
Molecular mass (kDa)	68	18.4
Net charge at pH 6	Negative	Negative

2.2 Nanoparticle characterization. The size and morphology of α-Fe_2O_3 nanoparticles were determined using a JEOL JEM-1400 Plus transmission electron microscopy (TEM) at 80 kV**.** For TEM imaging, a 10 μL droplet from a sonicated α-Fe_2O_3 nanoparticle suspension was deposited on a formvar/carbon-coated 100-mesh copper grid (Electron Microscopy Sciences) and kept inside a dry air chamber until it is completely dried. The exposed facet was further imaged with high-resolution TEM (JEOL-2800) at 200 kV. The crystalline phase of nanoparticles was determined using an APEX II Ultra diffractometer equipped with a CCD-based area detector, using MoK_α radiation at λ= 0.71073 Å. 2D images from the APEX II detector were processed using DiffractEva software (Bruker). A Quantachrome Nova 4200e analyzer was used to determine surface area and pore size via Brunauer-Emmett-Teller (BET) N_2 adsorption. Before BET analysis, samples were degassed for 8 hours at 120 ºC, and a 15 multipoint isotherm with partial pressures (P/P_o) of 0.05-0.95 was collected.

2.3 ATR-FTIR spectroscopy of protein adsorption and desorption reactions. ATR-FTIR spectroscopy was used to characterize the solution phase and adsorbed species. Protein solutions of 5 mg mL^{-1} native BSA and *β*-LG were prepared at pH 6. Two phosphate solutions of 25 mM and 250 μM were prepared for solution-phase analysis and adsorption studies, respectively. Aqueous protein spectra were collected using ATR-FTIR flow-cell crystal without an α-Fe_2O_3 coating. After the collection of protein solution spectra, a background spectrum of each solvent was subtracted from the sample spectrum. To reduce the interference of gas-phase water absorption bands, an atmospheric suppression correction was performed in the OMNIC 9 software (ThermoFisher).

Solution-phase spectra of the proteins were compared to those of protein adsorbates to observe any spectral changes that occur upon adsorption onto α-Fe_2O_3. The methodology for

surface adsorption and desorption steps is detailed in the Supporting Information (SI) Scheme S1. Briefly, experiments followed the following steps: (1) α-Fe_2O_3 nanoparticles were drop cast on the AMTIR crystal by depositing 1 mL of 5 mg mL^{-1} nanoparticle suspension; (2) dried overnight in a dry air chamber; (3) pH-adjusted (pH 6; 10 mM NaCl in Milli-Q water) salt solution flowed at 0.5 ml min^{-1} over the thin film for 20 min to remove any loosely bound nanoparticles, to adjust nanoparticle surface charge, and to allow for background spectra collection; (4) 250 μM phosphate buffer was introduced to the system for 90 min to create phosphate-coated nanoparticles before protein adsorption (this step was omitted in experiments lacking phosphate); (5) for each protein type, a continuous flow of a 1 mg mL^{-1} protein solution passed over the nanoparticle film surface for 90 min and; (6) a final flow of 10mM NaCl salt solution over the protein-coated surface for 90 min. Phosphate adsorption was confirmed by the observation of saturated adsorbed phosphate at ~90 min which was determined by plotting absorbance peak intensity for the adsorbed phosphate band (at 1040 cm^{-1}) during adsorption onto α-Fe_2O_3 (Fig. 2). pH was monitored and maintained at pH 6 throughout all experiments.

ATR-FTIR spectra were collected using a horizontal cell and an amorphous material transmitting infrared radiation (AMTIR) crystal (PIKE Technologies). The horizontal cell was placed inside of the internal compartment of a Thermo–Nicolet iS10 FTIR spectrometer equipped with a mercury cadmium telluride (MCT-A) detector with a lower wavenumber cutoff of 650 cm^{-1}. All spectra were recorded in 2-minute intervals at 4 cm^{-1} resolution, and an average of 128 scans was collected over the spectral range extending from 750 to 4000 cm^{-1}.

2.5 Curve-fitting analysis of the amide I band. To provide quantitative analyses of kinetic changes to protein secondary structures during adsorption, the amide I region of ATR-FTIR spectra was analyzed. Solution-phase conformations were compared to those of the adsorbed phase over

reaction-time and surface coverage. Selected time points of 4- and 90-minutes during adsorption were used to compare protein secondary structure at low and high surface coverage, respectively. Before curve fitting, the amide I band range (1600 to 1700 cm^{-1}) was baseline corrected and normalized to the highest peak intensity from each original time-dependent spectral series (Fig. S1). Second derivative spectra were obtained using Origin 2017 Suite (OriginLab Corporation, Northampton, Massachusetts, USA) to better resolve different vibrational peaks. The local minimum values from the second derivative of the ATR-FTIR spectra were used to identify band positions of the different secondary components and used for spectral assignments. Curve fitting iterations to a Gaussian shape at the band positions were then performed to achieve the best composite result. Protein solution-phase secondary structural results and previous literature values[26,35,52] were used for comparison to spectra of adsorbed proteins. Best fits were calculated within OriginLab using ANOVA-derived least squares regression analysis, and all R^2 values were found to be > 0.98.

3. Results and Discussion

3.1 Nanoparticle characterization. Fig. 1 shows the detailed physical characterization of iron oxide nanoparticles. From the XRD pattern in Fig. 1a, we verified that these nanoparticles were entirely hematite, with a specific surface area of 75.7 ± 8.2 m^2 g^{-1} and an average pore size of 0.247 cm^3 g^{-1} (Fig. S2). TEM and HRTEM images of α-Fe_2O_3 nanoparticles (Fig. 1b-c) indicated that the particles were aggregated and individual nanoparticles, albeit somewhat difficult to discern, appeared to be ca. 5 to 20 nm in diameter, in agreement with vendor specifications. High-resolution images, as shown in Fig. 1c, show that the most exposed facet was the (104) surface plane.

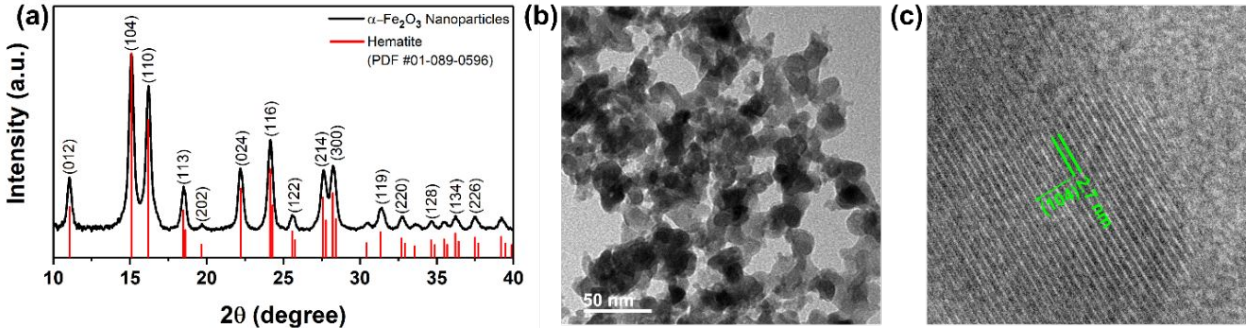

Figure 1. Characterization of α-Fe_2O_3 nanoparticles. (a) XRD pattern indicates that particles are hematite; (b) TEM and (c) HRTEM images of nanoparticles with an exposed (104) facet.

3.2 ATR-FTIR spectroscopy of phosphate in solution and adsorbed on α-Fe_2O_3. Solution-phase and adsorbed phosphate were both examined via ATR-FTIR spectroscopy to determine vibrational frequency changes. The protonation state of phosphate can be seen in Fig. S3a. At pH 6, the molar fraction of phosphate in solution is comprised of 0.94 $H_2PO_4^-$ and 0.06 HPO_4^{2-} (Fig. S3b). A representative ATR-FTIR spectrum is shown in Fig. S3c. There are two main phosphate (PO_4^{3-}) vibrations: nondegenerate symmetric stretch (ν_1) and triply degenerate asymmetric stretch (ν_3).[58,59] Due to asymmetry in the structure of the $H_2PO_4^-$ species, the bands at 990 cm^{-1} and 1155 cm^{-1} appear from the split degenerate asymmetric stretching band (ν_3). The absorption at 940 cm^{-1} is an indication of coexisting HPO_4^{2-} species and the ν_1 band is active at 878 cm^{-1}. The broad shoulder at ~1220 cm^{-1} represents bending mode [δ(POH)] and is derived from $H_2PO_4^-$ species.[58,59]

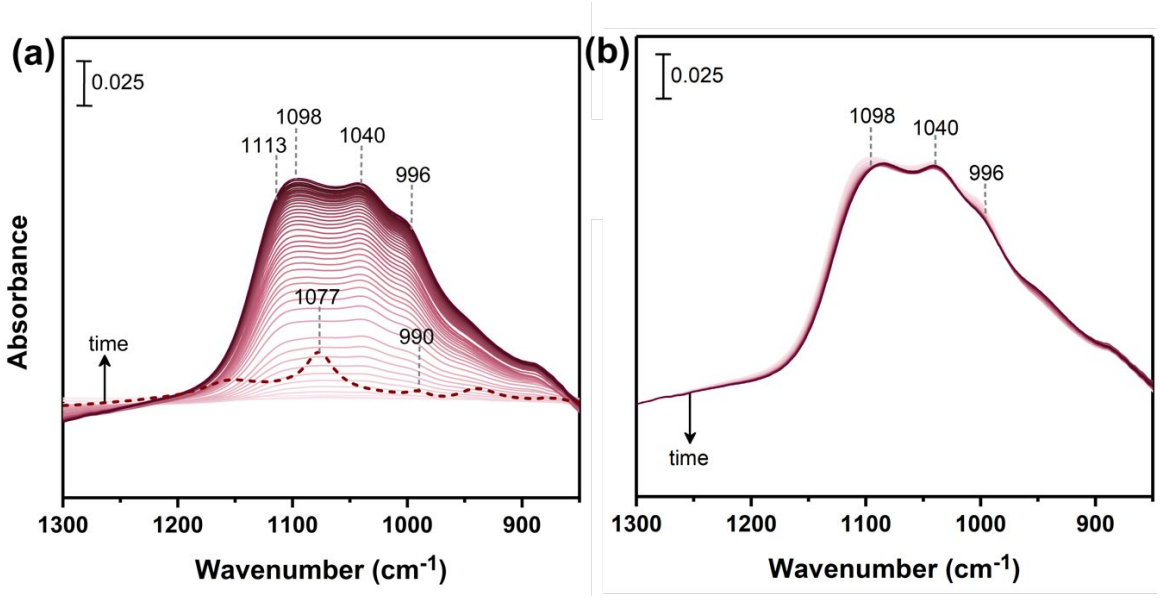

Figure 2. ATR-FTIR spectra of (a) 250 μM phosphate adsorption onto α-Fe_2O_3, and (b) following phosphate desorption from α-Fe_2O_3 with 10 mM NaCl, both as a function of time at pH 6. The dashed line in (a) represents the spectrum of 25 mM solution-phase phosphate in 10 mM NaCl solution at pH 6.

Adsorption and desorption spectra of phosphate were collected as a function of interaction time (Fig. 2). Phosphate adsorption onto α-Fe_2O_3 surfaces is shown in Fig. 2a. The bands observed ~1098 cm^{-1} and 1040 cm^{-1} are due to the P-O stretching vibration of the phosphate ion.[60] The absorption band region in Fig. 2a is quite broad, suggesting multiple adsorption bonding modes were co-occurring[58,61]. Normalized absorbance peak intensities of the adsorbed phosphate (using the band at 1040 cm^{-1}) during adsorption onto α-Fe_2O_3 (0-90 min) and desorption experiments (90-180 min) suggest that adsorbed phosphate reached equilibrium after ~90 min. Notably, Notably, phosphate was deemed to be irreversibly bound to the α-Fe_2O_3 surface, as the peak absorbance intensities did not change substantially when desorbed with 10 mM NaCl at pH 6 (Fig. 2b). This component of adsorbed phosphate may thus be bound via inner-sphere complexation directly at the solid-solution interface, as supported by the irreversibility of adsorption, in addition to physisorption interactions. These findings further support the occurrence of a mixture of surface species and bonding modes.[58,61,62]

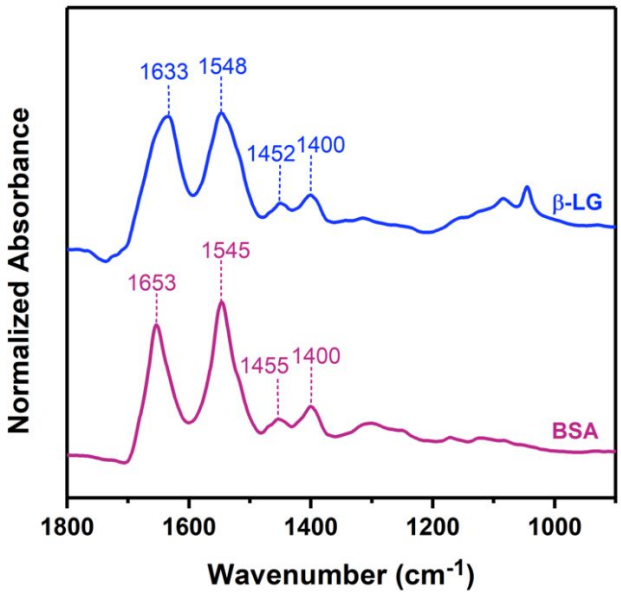

Figure 3. Normalized ATR-FTIR spectra of 5 mg mL^{-1} BSA and *β*-LG in 10 mM NaCl solution at pH 6. Spectra normalized by the Amide I band relative intensities. The peaks at 1633 cm^{-1} and 1653 cm^{-1} are for the Amide I bands; 1548 cm^{-1} and 1545 cm^{-1} peaks are for the amide II bands of the proteins. The peaks at 1452 cm^{-1} and 1455 cm^{-1} are assigned to the CH_2 scissoring, and 1400 cm^{-1} is from C–O carboxylate stretching. These peak assignments were further used to compare the solution phase with the adsorbed phase spectra in the amide I and II spectral regions.

3.3 ATR-FTIR spectroscopy of proteins in solution. ATR-FTIR spectra of BSA and *β*-LG solutions at pH 6 are shown in Fig. 3. The amide I bands were centered at 1633 cm^{-1} and 1653 cm^{-1} for *β*-LG and BSA, respectively.[35,51] The amide I band predominantly contains symmetric stretching of C=O, with contributions from out-of-phase C−N bending and in-plane N-H bending.[26,63] Amide II bands of the proteins were observed at 1548 cm^{-1} and 1545 cm^{-1} for *β*-LG and BSA, respectively.[36,51,52,64] The amide II and amide III (1200 to 1350 cm^{-1}) regions consist of out-of-phase C−N stretching and out-of-phase in-plane N-H bending from the peptide backbone of the proteins.[63,65] The peaks observed at 1452 cm^{-1} and 1455 cm^{-1} were assigned to CH_2 scissoring, and 1400 cm^{-1} was derived from C−O carboxylate groups. Peaks at approximately ~1050 cm^{-1}, observed in *β*-LG spectra, correspond to C−C and C−OH stretching modes.[65,66]

3.4 Kinetics of protein adsorption on α-Fe_2O_3 nanoparticle surfaces. After solution-phase characterization, BSA and *β*-LG were reacted with α-Fe_2O_3 nanoparticles in the presence and absence of phosphate, and temporal ATR-FTIR spectra were collected to investigate temporal adsorption dynamics (Fig. 4). For such kinetic analyses, changes to the amide II band were used to quantify protein adsorption, minimizing detection of potential aggregation and water interference.[29,67] Integration of peak intensities of the amide II band during protein adsorption revealed the presence of phosphate substantially dampened sorption rate and surface coverage of both BSA and *β*-LG on α-Fe_2O_3 nanoparticles (Fig. 4). Adsorbed BSA and *β*-LG concentrations were reduced by approximately 50% in the presence of phosphate, suggesting the latter is effectively competing for particle active sites. As α-Fe_2O_3 nanoparticles had a pH_{IEP} (isoelectric point) value near 6 during adsorption reactions (Fig. S2), indicating a neutral surface charge, electrostatic interactions with both negatively charged proteins are unfavorable and hydrogen bonding likely predominated.

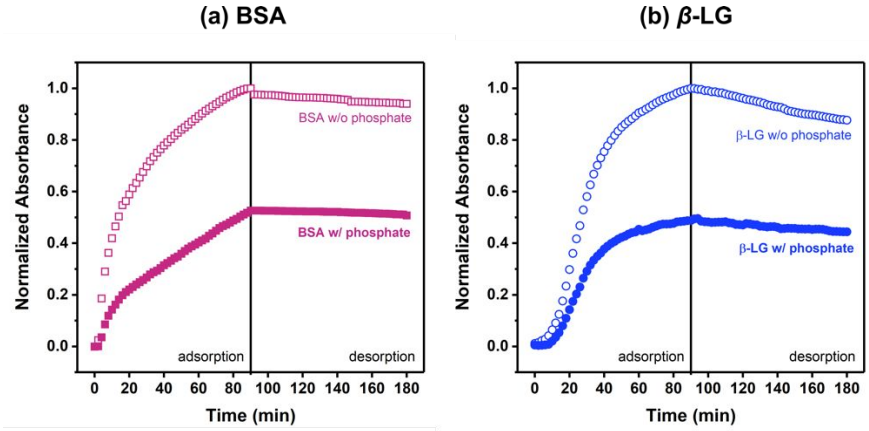

Figure 4. Normalized amide II peak absorbance of (a) BSA and (b) β-LG in the presence and absence of phosphate (closed and open markers, respectively) during α-Fe_2O_3 adsorption (0-90 min) and desorption (90-180 min).

These adsorption profiles revealed phosphate did not alter observed protein-specific kinetics substantially. BSA displayed potential Langmuir binding, although phosphate induced a

more linear adsorption profile, while *β*-LG exhibited a sigmoidal-shape (S-shape) adsorption curve (Fig. 4). Langmuir-type adsorption of BSA to oxides and clay materials has been commonly observed,[29,30,68] although many kinetic models display similar curve shapes and mechanistic details cannot be deduced. The difference in curve shape between protein is evident, however. In contrast, an S-shape adsorption profile is often caused by lateral interactions between adsorbed species and unrestricted monolayer-multilayer formation,[69–71] and may be driven by two-step cooperative binding, as shown by Hellner et al., 2019[72] in peptide adsorption to SiO_2. As each reaction system approached saturation, Amide I and II peak absorbance intensities of BSA and β-LG during adsorption were stable leading up to the 90 minute sampling, indicative of no change in secondary structures at this time point (Fig. S5).

To probe the reversibility of BSA and *β*-LG binding, desorption experiments were carried out by flowing 10 mM NaCl at pH 6 over protein-α-Fe_2O_3 nanoparticle complexes (Figs. 4, S4). Across all spectral regions (Fig. S4), both proteins exhibited low reversibility in the absence of phosphate, and greater partial desorption of *β*-LG supports the formation of a multilayer.[70] BSA desorption was not significantly altered in the presence of phosphate (Fig. S5a), while *β*-LG adsorption showed no loss of protein as well under the same conditions (Fig. S5b) suggesting multilayer formation was inhibited in the presence of phosphate.

3.5 Effect of pre-adsorbed phosphate on protein binding modes at the a-Fe_2O_3 interface. ATR-FTIR spectroscopy is a powerful *in-situ* characterization method to monitor protein binding mechanisms and secondary conformational changes upon adsorption onto nanoparticle surfaces.[73] As proteins adsorb to oxide surfaces and multidimensional structure emerges, protein binding environments, conformation, and aggregation change dynamically.[57,74,75] The presence of co-adsorbates, such as phosphate, may modulate protein coordination and structure through

competition and subsequent steric constraints. Thus, to understand the impact of phosphate on protein conformation, IR spectra of adsorbed BSA and *β*-LG were collected with and without pre-adsorbed phosphate. To identify specific surface interactions causing frequency shifts and band shape differences, solution-phase spectral results (Fig. 3) were compared to those of adsorbed species (Fig. 5).

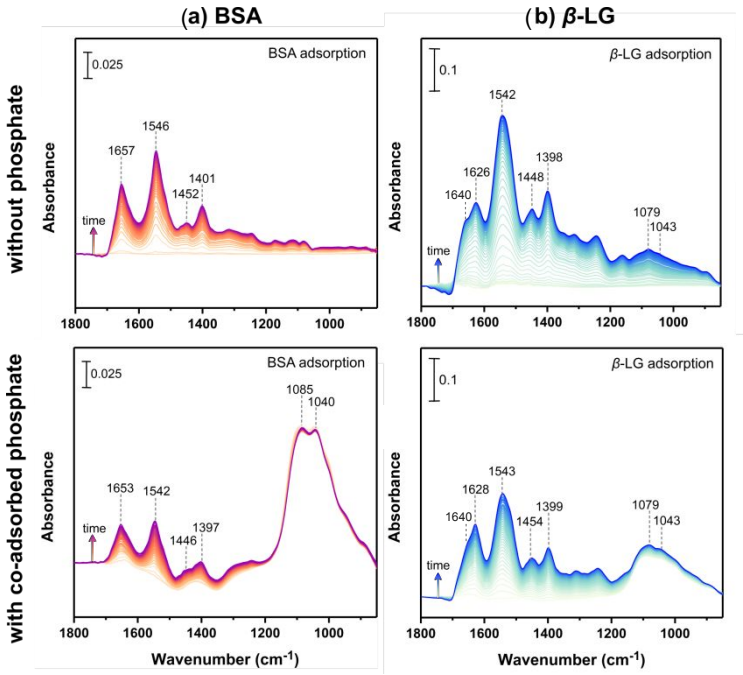

Figure 5. ATR-FTIR spectra of 1 mg mL^{-1} (a) BSA and (b) *β*-LG adsorption onto α-Fe_2O_3 nanoparticles without phosphate (top) and with pre-adsorbed phosphate (bottom) as a function of time (color scale).

Compared to solution-phase spectra, shifts in vibrational frequencies upon adsorption indicate inner-sphere coordination, secondary structural changes, and hydrogen bonding interactions between the protein and nanoparticle surface.[64] Specifically, secondary structural changes can be observed by changes in the frequencies and absorption band shapes of both the amide I and amide II bands of BSA and *β*-LG spectra. The vibrational frequency assignments for these bands are given in Table 2. Structural changes were protein-specific: frequency shifts from BSA adsorption were minimal, particularly in the presence of phosphate, suggesting induction of

only small structural changes, while *β*-LG adsorption was marked by larger shifts to lower wavenumbers. Such shifts in the amide I band have been suggested to be indicative of increasing hydrogen bonds.[63] The presence of phosphate dampened this shift, which has been proposed to indicate a subsequent conformational change, and thus pre-adsorbed phosphate may reduce the extent of protein secondary structural changes and prevent protein denaturation on the α-Fe_2O_3 surface.

Table 2. Vibrational frequencies for protein amide I and amide II peaks in solution phase and upon adsorption on α-Fe_2O_3 nanoparticle surfaces at pH 6.

	Vibrational Frequency (cm^{-1})					
	BSA			***β*-LG**		
	Solution Phase	**Adsorbed on α-Fe_2O_3 (Δ)***	**Adsorbed on phosphate-coated α-Fe_2O_3 (Δ)***	**Solution Phase**	**Adsorbed on α-Fe_2O_3 (Δ)***	**Adsorbed on phosphate-coated α-Fe_2O_3 (Δ)***
Amide I	1653	1657 (+4)	1653 (0)	1633	1626 (-7)	1628 (-5)
Amide II	1545	1546 (+1)	1542 (-3)	1548	1542 (-6)	1543 (-5)

(Δ)* = Difference between adsorbed and solution-phase vibrational frequency.

Reductions in *β*-LG hydrogen bonding in the presence of phosphate were further supported by changes in amide band shapes. When *β*-LG was adsorbed in the absence of phosphate, the spectral shoulder at 1640 cm^{-1} developed (Fig. 5b), which has been suggested to be due to hydrogen bonding changes upon protein adsorption.[63] However, in the presence of phosphate, the band shape of *β*-LG amide I resembled its shape in the solution phase, indicating co-adsorbed phosphate constrained protein denaturation and secondary structural changes.[26] Notably, we observed no change in phosphate band intensities during sorption experiments; however, band shape changes were detected upon protein introduction, indicating possible differences in surface phosphate species present on the surface as well as different modes of binding to the surface when co-adsorbed protein was present (Fig. S4).

3.6 Secondary structural analyses of adsorbed proteins. Protein secondary structures were further investigated, leveraging both changes in the amide I/II ratio over time and curve-fitting of the amide I band, which is highly sensitive to protein conformational changes.[32] Initial analysis of temporal changes in the amide I/II ratio reveals time-dependent, phosphate-driven protein conformational changes during adsorption (Fig. S5).[76] Reduced ratios indicates that protein conformational changes occurring in the first 20 minutes in the absence of phosphate, whereas the conformational change occurred over 60 minutes in the presence of co-adsorbed phosphate, as can be seen by the steady ratio after this time. These observations were used to select time points for secondary structural analysis at early (4 minutes) and later (90 minutes) reaction times.

Using a curve-fitting approach, protein solution-phase and adsorbed ATR-FTIR spectra were deconvoluted into β-sheets, turns, α-helices, extended chains (short-segment chains connecting the α-helical segment), random coils, and side-chain moieties (Fig. S6). Vibrational frequencies (cm^{-1}) of the solution and adsorbed peak centers associated with individual secondary structure components of the BSA and β-LG solutions after curve fitting are summarized in Table S1. The peak center positions were shifted ±3 cm^{-1} from the local minimum positions determined by the second derivative, and the coefficients of determination (R^2) were ≥ 0.9 for deconvolution fits. Unreacted solution-phase spectra of β-LG indicate its structure is comprised of a short α-helix and eight strands of antiparallel β-sheets, which form a conical barrel.[33] In contrast, BSA has been shown to be comprised solely of α-helix structures.[35] However, it is essential to note that reported variations are possible within ±10% among secondary structures distribution.[10] Our curve-fitting results for solution-phase protein conformational analyses, shown in Fig. S6, were aligned with previous findings[35], as the dominant component of the BSA solution-phase conformation at pH 6

was largely α-helix (52%), while the *β*-LG solution was primarily comprised of extended chains/β-sheets (49%).

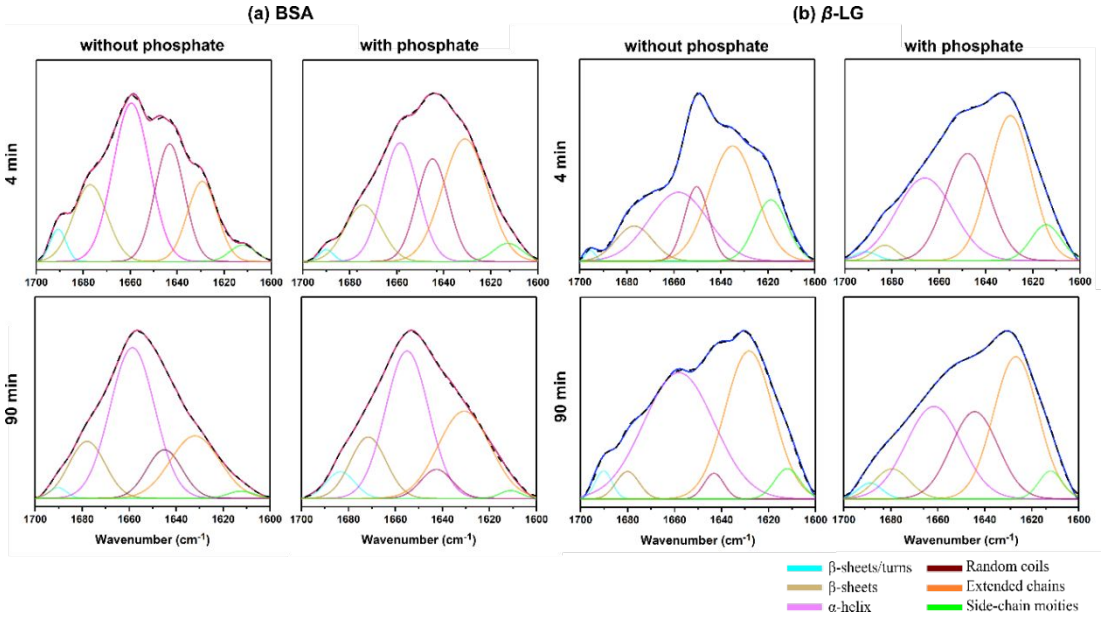

Figure 6. Background subtracted and normalized protein amide I band for secondary structural analysis with curve fitting results for (a) BSA and (b) *β*-LG adsorbed on α-Fe_2O_3 nanoparticles in the presence and absence of pre-adsorbed phosphate at pH 6.0. The magenta and dark blue solid lines represent the original experimental spectrum, and the black dashed lines represent the cumulative fit. Component bands are given for intermolecular β-sheets/turns (cyan), β-sheets (green/brown), α-helices (fuchsia), random coils (dark red), short-segment chains connecting the α-helices (orange), side-chain moieties (lime).

Changes in these relative spectral contributions during protein adsorption to α-Fe_2O_3 nanoparticles at 4- and 90-minutes were used to further our understanding of the dynamic effects of pre-adsorbed phosphate on adsorbed protein conformation (Fig. 6, Table 3).[35,65,77,78] Initial adsorption (4 minutes) in the absence of phosphate induced structural changes in both proteins compared to solution-phase conformations (Fig. S6), as BSA underwent a gain in extended chains (+18%) while *β*-LG exhibited increasing α-helix (+19%) and decreasing random coil (-26%) content (Table 3). The suggested unfolding process after BSA adsorption on metal oxides has been previously observed,[26,35] as has the formation of non-native α-helical *β*-LG intermediates in complex systems, as the amino acid sequence of *β*-LG has a markedly high preference for an α-helix conformation.[79] The observed increase in relative alpha helix abundance, however, may also

be due to the relative preferential unfolding in β sheets. When phosphate was present, transformations were substantially reduced. Phosphate may inhibit adsorptive protein conformational changes through bridging and ternary complex formation[80–82] or induction of steric constraints. These results are in agreement with studies on other oxide surfaces, such as TiO_2, where phosphate attenuates conformational changes of proteins. Although the degree to which these structural changes occur within BSA, in the presence or absence of phosphate, depends on the specific phase and size of the nanoparticle, the impact of adsorbed phosphate in modulating changes in the protein structure appears to be quite similar between different oxides (α-Fe_2O_3 and TiO_2) and different sizes/phases of TiO_2.[26,64]

Table 3. Secondary structural elements content (%) in the amide I region, determined via curve-fitting for solution phase (5 mg/mL) and after 90 min adsorption onto α-Fe_2O_3 and phosphate-coated α-Fe_2O_3.

			Adsorbed on α-Fe_2O_3 (Δ)*		**Adsorbed on phosphate-coated α-Fe_2O_3 (Δ)***	
	Secondary Structure	**Solution Phase**	**4 min**	**90 min**	**4 min**	**90 min**
BSA	β-sheets/turns	3	3 (0)	5 (+2)	1 (-2)	1 (-2)
	β-sheets	20	17 (-3)	15 (-5)	13 (-7)	15 (-15)
	α-helices	52	38 (-14)	43 (-9)	27 (-25)	48 (-4)
	Random coils	11	23 (+12)	6 (+5)	21 (+10)	12 (+1)
	Extended chains	12	15 (+3)	30 (+18)	35 (+13)	22 (+10)
	Side-chain moieties	2	4 (+2)	1 (+1)	3 (+1)	2 (0)
	Secondary Structure	**Solution Phase**	**4 min**	**90 min**	**4 min**	**90 min**
***β*-LG**	β-sheets/turns	4	1 (-3)	3 (+1)	1 (-3)	2 (-2)
	β-sheets	13	9 (-4)	3 (+10)	2 (-11)	6 (-7)
	α-helices	19	27 (+8)	48 (+29)	27 (+8)	29 (+9)
	Random coils	29	12 (-17)	3 (-26)	28 (-1)	23 (-6)
	Extended chains	32	37 (-5)	39 (+7)	35 (+3)	36 (+4)
	Side-chain moieties	3	14 (+11)	4 (+1)	7 (+4)	4 (+1)

(Δ)* = Difference between adsorbed and solution phase secondary structure content.

After 90 minutes (Fig. 6), both proteins approached solution-phase conformations (Fig. S6), regardless of phosphate. Smaller changes, such as the persistence of random coils in the *β*-LG

phosphate system, were observed, but composite spectra were highly consistent with those observed before adsorption. Broadly, this temporal evolution suggests significant protein conformational changes occurred at low surface coverage (4 minutes), and native conformations were reassumed at higher coverage (90 minutes) These results are in agreement with analyses of the amide I/II ratio shown in Fig. S5. The observation of solution-phase conformation at 90 min may be due to re-folding as additional proteins adsorb, or a scaffolding of unchanged proteins onto altered inner-layer proteins to the extent that the observable signature is dominantly of the unaltered, solution-phase conformation. While few studies have examined the effect of phosphate on oxide biomolecule adsorption, prior work by Xu et al. investigating pH effects on BSA complexation with TiO_2 observed similar conformations at pH 7.4 after 90 minutes of reaction time. Both adsorption reaction sets, in the presence and absence of phosphate, were also found to be irreversible. This suggests that our observations of phosphate-mediated inhibition of adsorption rates and conformational changes are not specific to α-Fe_2O_3 nanoparticles, but likely rather driven by the presence of adsorbed phosphate. Thus, we propose for oxide surfaces in general that protein adsorption and structure in the environment are impacted by oxyanions, in particular phosphate.

4. Conclusions

Solution and temporal solid-phase ATR-FTIR spectroscopic measurements demonstrate the impact of phosphate on protein adsorption kinetics, coverage, and conformation at nanoscale oxide interfaces. Phosphate pre-adsorption to α-Fe_2O_3 nanoparticles slowed both β-LG and BSA adsorption kinetics, which were observed to be protein-specific, and resulted in an approximately 50% reduction in protein surface coverage. BSA was observed to exhibit Langmuir-like kinetic curves, while contrastingly β-LG showed potentially two-step adsorption dynamics, suggesting

that directly-coordinated BSA may be less bioavailable than *β*-LG. Deconvolution analyses of ATR-FTIR spectra at low- and high-coverage conditions revealed initial changes in both *β*-LG and BSA secondary conformation, despite longstanding consideration of *β*-LG as a rigid protein, followed by a return to solution-phase conformation at 90 minutes, approaching saturation. BSA unfolded into random coils and extended chains, while *β*-LG transitioned into primarily α-helix structures. Importantly, phosphate markedly reduced these early conformational changes and thus may serve as an effective modulator of adsorbed protein function, particularly at low surface coverage. Such conditions are highly relevant for many environmental matrices, where reported protein concentrations in solution range from 1 to 100 mg L^{-1}. Our work suggests that adsorption to oxide nanoparticles and associated conformational changes may render enzymes inactive in these systems, and highlights the importance of phosphate in attenuating protein denaturation in environmental and industrial applications, such as environmental safety, remediation, and ecosystem health. These results contribute to a growing understanding and future investigations of complex protein coronae formation at environmental interfaces[86].

5. Acknowledgments

The research reported here was funded in whole or in part by the Army Research Office/Army Research Laboratory via grant #W911NF-19-1-0078 to the University of California, San Diego. Any errors and opinions are not those of the Army Research Office or Department of Defense and are attributable solely to the author(s). FE-SEM imaging was performed in part at the San Diego Nanotechnology Infrastructure (SDNI) of UCSD, a member of the National Nanotechnology Coordinated Infrastructure, supported by the NSF (Grant ECCS-1542148). The authors thank Dr. Haibin Wu for helpful discussions and for performing HR-TEM imaging.

6. References

(1) Cornell, R. M.; Schwertmann, U. Introduction to the Iron Oxides. In *The Iron Oxides*; **2003**. https://doi.org/10.1002/3527602097.ch1.

(2) Hochella, M. F.; Lower, S. K.; Maurice, P. A.; Penn, R. L.; Sahai, N.; Sparks, D. L.; Twining, B. S. Nanominerals, Mineral Nanoparticles, and Earth Systems. *Science*. 2008. https://doi.org/10.1126/science.1141134.

(3) Theng, B. K. G.; Yuan, G. Nanoparticles in the Soil Environment. *Elements* **2008**. https://doi.org/10.2113/gselements.4.6.395.

(4) Keller, A. A.; McFerran, S.; Lazareva, A.; Suh, S. Global Life Cycle Releases of Engineered Nanomaterials. *J. Nanoparticle Res.* **2013**. https://doi.org/10.1007/s11051-013-1692-4.

(5) Schwaminger, S. P.; Fraga-García, P.; Selbach, F.; Hein, F. G.; Fu, E. C.; Surya, R.; Roth, H. C.; Blank-Shim, S. A.; Wagner, F. E.; Heissler, S.; et al. Bio-Nano Interactions: Cellulase on Iron Oxide Nanoparticle Surfaces. *Adsorption* **2017**. https://doi.org/10.1007/s10450-016-9849-y.

(6) Waychunas, G. A.; Kim, C. S.; Banfield, J. F. Nanoparticulate Iron Oxide Minerals in Soils and Sediments: Unique Properties and Contaminant Scavenging Mechanisms. In *Journal of Nanoparticle Research*; **2005**. https://doi.org/10.1007/s11051-005-6931-x.

(7) Bolisetty, S.; Vallooran, J. J.; Adamcik, J.; Mezzenga, R. Magnetic-Responsive Hybrids of Fe_3O_4 Nanoparticles with β-Lactoglobulin Amyloid Fibrils and Nanoclusters. *ACS Nano* **2013**. https://doi.org/10.1021/nn401988m.

(8) Mudunkotuwa, I. A.; Grassian, V. H. The Devil Is in the Details (or the Surface): Impact of Surface Structure and Surface Energetics on Understanding the Behavior of Nanomaterials in the Environment. *Journal of Environmental Monitoring* **2011**. https://doi.org/10.1039/c1em00002k.

(9) Limo, M. J.; Sola-Rabada, A.; Boix, E.; Thota, V.; Westcott, Z. C.; Puddu, V.; Perry, C. C. Interactions between Metal Oxides and Biomolecules: From Fundamental Understanding to Applications. *Chemical Reviews* **2018**. https://doi.org/10.1021/acs.chemrev.7b00660.

(10) Barreto, M. S. C.; Elzinga, E. J.; Alleoni, L. R. F. The Molecular Insights into Protein Adsorption on Hematite Surface Disclosed by In-Situ ATR-FTIR/2D-COS Study. *Sci. Rep.* **2020**, *10* (1), 1–13. https://doi.org/10.1038/s41598-020-70201-z.

(11) Mazeina, L.; Navrotsky, A. Enthalpy of Water Adsorption and Surface Enthalpy of Goethite (α-FeOOH) and Hematite (α-Fe2O3). *Chem. Mater.* **2007**. https://doi.org/10.1021/cm0623817.

(12) Alberts, B.; Bray, D.; Johnson, A.; Lewis, J.; Raff, M.; Roberts, K.; Walter, P.; Alberts,

B.; Bray, D.; Johnson, A.; et al. Protein Structure and Function. In *Essential Cell Biolog*; **2018**. https://doi.org/10.1201/9781315815015-4.

(13) Enzymes in the Environment: Activity, Ecology, and Applications. *Choice Rev. Online* **2002**. https://doi.org/10.5860/choice.40-1527.

(14) Littlechild, J. A. Protein Structure and Function. In *Introduction to Biological and Small Molecule Drug Research and Development: Theory and Case Studies* **2013**. https://doi.org/10.1016/B978-0-12-397176-0.00002-9.

(15) Alberts, B.; A, J.; Lewis J. Analyzing Protein Structure and Function. *Mol. Biol. Cell* **2002**.

(16) Newcomb, C. J.; Qafoku, N. P.; Grate, J. W.; Bailey, V. L.; De Yoreo, J. J. Developing a Molecular Picture of Soil Organic Matter-Mineral Interactions by Quantifying Organo-Mineral Binding. *Nat. Commun.* **2017**. https://doi.org/10.1038/s41467-017-00407-9.

(17) Moon, J.; Xia, K.; Williams, M. A. Consistent Proteinaceous Organic Matter Partitioning into Mineral and Organic Soil Fractions during Pedogenesis in Diverse Ecosystems. *Biogeochemistry* **2019**. https://doi.org/10.1007/s10533-018-0523-1.

(18) Kim, J. T.; Weber, N.; Shin, G. H.; Huang, Q.; Liu, S. X. The Study of β-Lactoglobulin Adsorption on Polyethersulfone Thin Film Surface Using QCM-D and AFM. *J. Food Sci.* **2007**. https://doi.org/10.1111/j.1750-3841.2007.00344.

(19) Rabe, M.; Verdes, D.; Seeger, S. Understanding Protein Adsorption Phenomena at Solid Surfaces. *Advances in Colloid and Interface Science* **2011**. https://doi.org/10.1016/j.cis.2010.12.007.

(20) Casals, E.; Pfaller, T.; Duschl, A.; Oostingh, G. J.; Puntes, V. Time Evolution of the Nanoparticle Protein Corona. *ACS Nano* **2010**. https://doi.org/10.1021/nn901372t.

(21) Lynch, I.; Dawson, K. A. Protein-Nanoparticle Interactions. *Nano Today* **2008**. https://doi.org/10.1016/S1748-0132(08)70014-8.

(22) Nasser, F.; Constantinou, J.; Lynch, I. Nanomaterials in the Environment Acquire an "Eco-Corona" Impacting Their Toxicity to Daphnia Magna—a Call for Updating Toxicity Testing Policies. *Proteomics* **2020**. https://doi.org/10.1002/pmic.201800412.

(23) Mei, N.; Hedberg, J.; Odnevall Wallinder, I.; Blomberg, E. Influence of Biocorona Formation on the Transformation and Dissolution of Cobalt Nanoparticles under Physiological Conditions. *ACS Omega* **2019**. https://doi.org/10.1021/acsomega.9b02641.

(24) Liu, F.; Li, X.; Sheng, A.; Shang, J.; Wang, Z.; Liu, J. Kinetics and Mechanisms of Protein Adsorption and Conformational Change on Hematite Particles. *Environ. Sci. Technol.* **2019**. https://doi.org/10.1021/acs.est.9b02651.

(25) Nielsen, K. M.; Calamai, L.; Pietramellara, G. Stabilization of Extracellular DNA and

Proteins by Transient Binding to Various Soil Components. In *Nucleic Acids and Proteins in Soil* **2006**. https://doi.org/10.1007/3-540-29449-x_7.

(26) Xu, Z.; Grassian, V. H. Bovine Serum Albumin Adsorption on TiO_2 Nanoparticle Surfaces: Effects of Ph and Coadsorption of Phosphate on Protein-Surface Interactions and Protein Structure. *J. Phys. Chem. C* **2017**. https://doi.org/10.1021/acs.jpcc.7b07525.

(27) Satzer, P.; Svec, F.; Sekot, G.; Jungbauer, A. Protein Adsorption onto Nanoparticles Induces Conformational Changes: Particle Size Dependency, Kinetics, and Mechanisms. *Eng. Life Sci.* **2016**. https://doi.org/10.1002/elsc.201500059.

(28) Schmidt, M. P.; Martínez, C. E. Supramolecular Association Impacts Biomolecule Adsorption onto Goethite. *Environ. Sci. Technol.* **2018**. https://doi.org/10.1021/acs.est.7b06173.

(29) Schmidt, M. P.; Martínez, C. E. Kinetic and Conformational Insights of Protein Adsorption onto Montmorillonite Revealed Using in Situ ATR-FTIR/2D-COS. *Langmuir* **2016**, *32* (31), 7719–7729. https://doi.org/10.1021/acs.langmuir.6b00786.

(30) Andersen, A.; Reardon, P. N.; Chacon, S. S.; Qafoku, N. P.; Washton, N. M.; Kleber, M. Protein-Mineral Interactions: Molecular Dynamics Simulations Capture Importance of Variations in Mineral Surface Composition and Structure. *Langmuir* **2016**, *32* (24), 6194–6209. https://doi.org/10.1021/acs.langmuir.6b01198.

(31) Ustunol, I. B.; Gonzalez-Pech, N. I.; Grassian, V. H. PH-Dependent Adsorption of α-Amino Acids, Lysine, Glutamic Acid, Serine and Glycine, on TiO2 Nanoparticle Surfaces. *J. Colloid Interface Sci.* **2019**, *554*, 362–375. https://doi.org/10.1016/j.jcis.2019.06.086.

(32) Roach, P.; Farrar, D.; Perry, C. C. Interpretation of Protein Adsorption: Surface-Induced Conformational Changes. *J. Am. Chem. Soc.* **2005**. https://doi.org/10.1021/ja042898o.

(33) Assifaoui, A.; Huault, L.; Maissiat, C.; Roullier-Gall, C.; Jeandet, P.; Hirschinger, J.; Raya, J.; Jaber, M.; Lambert, J. F.; Cayot, P.; et al. Structural Studies of Adsorbed Protein (Betalactoglobulin) on Natural Clay (Montmorillonite). *RSC Adv.* **2014**. https://doi.org/10.1039/c4ra11607k.

(34) Kolman, K.; Makowski, M. M.; Golriz, A. A.; Kappl, M.; Pigłowski, J.; Butt, H. J.; Kiersnowski, A. Adsorption, Aggregation, and Desorption of Proteins on Smectite Particles. *Langmuir* **2014**. https://doi.org/10.1021/la502840s.

(35) Givens, B. E.; Xu, Z.; Fiegel, J.; Grassian, V. H. Bovine Serum Albumin Adsorption on SiO_2 and TiO_2 Nanoparticle Surfaces at Circumneutral and Acidic PH: A Tale of Two Nano-Bio Surface Interactions. *J. Colloid Interface Sci.* **2017**. https://doi.org/10.1016/j.jcis.2017.01.011.

(36) Sit, I.; Xu, Z.; Grassian, V. H. Plasma Protein Adsorption on TiO_2 Nanoparticles: Impact of Surface Adsorption on Temperature-Dependent Structural Changes. *Polyhedron* **2019**,

171, 147–154. https://doi.org/10.1016/j.poly.2019.06.036.

(37) Basu, M. K.; Poliakov, E.; Rogozin, I. B. Domain Mobility in Proteins: Functional and Evolutionary Implications. *Brief. Bioinform.* **2009**. https://doi.org/10.1093/bib/bbn057.

(38) Pérez-Fuentes, L.; Drummond, C.; Faraudo, J.; Bastos-González, D. Adsorption of Milk Proteins (β-Casein and β-Lactoglobulin) and BSA onto Hydrophobic Surfaces. *Materials (Basel).* **2017**. https://doi.org/10.3390/ma10080893.

(39) Fadare, O. O.; Wan, B.; Liu, K.; Yang, Y.; Zhao, L.; Guo, L.-H. Eco-Corona vs Protein Corona: Effects of Humic Substances on Corona Formation and Nanoplastic Particle Toxicity in Daphnia Magna . *Environ. Sci. Technol.* **2020**. https://doi.org/10.1021/acs.est.0c00615.

(40) Kleber, M.; Sollins, P.; Sutton, R. A Conceptual Model of Organo-Mineral Interactions in Soils: Self-Assembly of Organic Molecular Fragments into Zonal Structures on Mineral Surfaces. *Biogeochemistry* **2007**. https://doi.org/10.1007/s10533-007-9103-5.

(41) Coward, E. K.; Ohno, T.; Sparks, D. L. Direct Evidence for Temporal Molecular Fractionation of Dissolved Organic Matter at the Iron Oxyhydroxide Interface. *Environ. Sci. Technol.* **2019**. https://doi.org/10.1021/acs.est.8b04687.

(42) Leinemann, T.; Preusser, S.; Mikutta, R.; Kalbitz, K.; Cerli, C.; Höschen, C.; Mueller, C. W.; Kandeler, E.; Guggenberger, G. Multiple Exchange Processes on Mineral Surfaces Control the Transport of Dissolved Organic Matter through Soil Profiles. *Soil Biol. Biochem.* **2018**. https://doi.org/10.1016/j.soilbio.2017.12.006.

(43) Saptarshi, S. R.; Duschl, A.; Lopata, A. L. Interaction of Nanoparticles with Proteins: Relation to Bio-Reactivity of the Nanoparticle. *J. Nanobiotechnology* **2013**. https://doi.org/10.1186/1477-3155-11-26.

(44) Vroman, L. Effect of Adsorbed Proteins on the Wettability of Hydrophilic and Hydrophobic Solids. *Nature* **1962**. https://doi.org/10.1038/196476a0.

(45) Holtan, H.; Kamp-Nielsen, L.; Stuanes, A. O. Phosphorus in Soil, Water and Sediment: An Overview. *Hydrobiologia* **1988**. https://doi.org/10.1007/BF00024896.

(46) Holman, I. P.; Whelan, M. J.; Howden, N. J. K.; Bellamy, P. H.; Willby, N. J.; Rivas-Casado, M.; McConvey, P. Phosphorus in Groundwater - An Overlooked Contributor to Eutrophication? *Hydrol. Process.* **2008**. https://doi.org/10.1002/hyp.7198.

(47) Zhao, G.; Du, J.; Jia, Y.; Lv, Y.; Han, G.; Tian, X. The Importance of Bacteria in Promoting Algal Growth in Eutrophic Lakes with Limited Available Phosphorus. *Ecol. Eng.* **2012**. https://doi.org/10.1016/j.ecoleng.2012.02.007.

(48) Wei, T.; Kaewtathip, S.; Shing, K. Buffer Effect on Protein Adsorption at Liquid/Solid Interface. *J. Phys. Chem. C* **2009**. https://doi.org/10.1021/jp806586n.

(49) Huang, X. Intersection of Isotherms for Phosphate Adsorption on Hematite. *J. Colloid Interface Sci.* **2004**. https://doi.org/10.1016/j.jcis.2003.12.007.

(50) Moulton, S. E.; Barisci, J. N.; McQuillan, A. J.; Wallace, G. G. ATR-IR Spectroscopic Studies of the Influence of Phosphate Buffer on Adsorption of Immunoglobulin G to TiO2. *Colloids Surfaces A Physicochem. Eng. Asp.* **2003**. https://doi.org/10.1016/S0927-7757(03)00078-5.

(51) O'Loughlin, I. B.; Kelly, P. M.; Murray, B. A.; Fitzgerald, R. J.; Brodkorb, A. Concentrated Whey Protein Ingredients: A Fourier Transformed Infrared Spectroscopy Investigation of Thermally Induced Denaturation. *Int. J. Dairy Technol.* **2015**. https://doi.org/10.1111/1471-0307.12239.

(52) Fang, Y.; Dalgleish, D. G. Conformation of β-Lactoglobulin Studied by FTIR: Effect of PH, Temperature, and Adsorption to the Oil-Water Interface. *J. Colloid Interface Sci.* **1997**. https://doi.org/10.1006/jcis.1997.5191.

(53) Ehn, B. M.; Ekstrand, B.; Bengtsson, U.; Ahlstedt, S. Modification of IgE Binding during Heat Processing of the Cow's Milk Allergen β-Lactoglobulin. *J. Agric. Food Chem.* **2004**. https://doi.org/10.1021/jf0304371.

(54) Krebs, M. R. H.; Devlin, G. L.; Donald, A. M. Amyloid Fibril-like Structure Underlies the Aggregate Structure across the pH Range for β-Lactoglobulin. *Biophys. J.* **2009**. https://doi.org/10.1016/j.bpj.2009.03.028.

(55) Bouhekka, A.; Bürgi, T. In Situ ATR-IR Spectroscopy Study of Adsorbed Protein: Visible Light Denaturation of Bovine Serum Albumin on TiO_2. *Appl. Surf. Sci.* **2012**. https://doi.org/10.1016/j.apsusc.2012.08.017.

(56) Madden, A. S.; Hochella, M. F.; Luxton, T. P. Insights for Size-Dependent Reactivity of Hematite Nanomineral Surfaces through Cu^{2+} Sorption. *Geochim. Cosmochim. Acta* **2006**, *70* (16), 4095–4104. https://doi.org/10.1016/j.gca.2006.06.1366.

(57) Rodzik, A.; Pomastowski, P.; Sagandykova, G. N.; Buszewski, B. Interactions of Whey Proteins with Metal Ions. *International Journal of Molecular Sciences*. 2020. https://doi.org/10.3390/ijms21062156.

(58) Elzinga, E. J.; Sparks, D. L. Phosphate Adsorption onto Hematite: An in Situ ATR-FTIR Investigation of the Effects of PH and Loading Level on the Mode of Phosphate Surface Complexation. *J. Colloid Interface Sci.* **2007**. https://doi.org/10.1016/j.jcis.2006.12.061.

(59) Tejedor-Tejedor, M. I.; Anderson, M. A. Protonation of Phosphate on the Surface of Goethite As Studied by CIR-FTIR and Electrophoretic Mobility. *Langmuir* **1990**. https://doi.org/10.1021/la00093a015.

(60) Gong, W. A Real Time in Situ ATR-FTIR Spectroscopic Study of Linear Phosphate Adsorption on Titania Surfaces. *Int. J. Miner. Process.* **2001**. https://doi.org/10.1016/S0301-7516(01)00045-X.

(61) Kubicki, J. D.; Paul, K. W.; Kabalan, L.; Zhu, Q.; Mrozik, M. K.; Aryanpour, M.; Pierre-Louis, A. M.; Strongin, D. R. ATR-FTIR and Density Functional Theory Study of the Structures, Energetics, and Vibrational Spectra of Phosphate Adsorbed onto Goethite. *Langmuir* **2012**. https://doi.org/10.1021/la303111a.

(62) Arai, Y.; Sparks, D. L. ATR-FTIR Spectroscopic Investigation on Phosphate Adsorption Mechanisms at the Ferrihydrite-Water Interface. *J. Colloid Interface Sci.* **2001**. https://doi.org/10.1006/jcis.2001.7773.

(63) Barth, A. Infrared Spectroscopy of Proteins. *Biochimica et Biophysica Acta - Bioenergetics*. 2007. https://doi.org/10.1016/j.bbabio.2007.06.004.

(64) Kim, J.; Doudrick, K. Emerging Investigator Series: Protein Adsorption and Transformation on Catalytic and Food-Grade TiO_2 Nanoparticles in the Presence of Dissolved Organic Carbon. *Environ. Sci. Nano* **2019**. https://doi.org/10.1039/c9en00130a.

(65) Givens, B. E.; Diklich, N. D.; Fiegel, J.; Grassian, V. H. Adsorption of Bovine Serum Albumin on Silicon Dioxide Nanoparticles: Impact of p H on Nanoparticle–Protein Interactions . *Biointerphases* **2017**. https://doi.org/10.1116/1.4982598.

(66) Gbassi, G.; Yolou, F.; Sarr, S.; Atheba, P.; Amin, C.; Ake, M. Whey Proteins Analysis in Aqueous Medium and in Artificial Gastric and Intestinal Fluids. *Int. J. Biol. Chem. Sci.* **2012**. https://doi.org/10.4314/ijbcs.v6i4.38.

(67) Tsai, D. H.; Delrio, F. W.; Keene, A. M.; Tyner, K. M.; MacCuspie, R. I.; Cho, T. J.; Zachariah, M. R.; Hackley, V. A. Adsorption and Conformation of Serum Albumin Protein on Gold Nanoparticles Investigated Using Dimensional Measurements and in Situ Spectroscopic Methods. *Langmuir* **2011**. https://doi.org/10.1021/la104124d.

(68) Song, L.; Yang, K.; Jiang, W.; Du, P.; Xing, B. Adsorption of Bovine Serum Albumin on Nano and Bulk Oxide Particles in Deionized Water. *Colloids Surfaces B Biointerfaces* **2012**, *94*, 341–346. https://doi.org/10.1016/j.colsurfb.2012.02.011.

(69) Scheufele, F. B.; Módenes, A. N.; Borba, C. E.; Ribeiro, C.; Espinoza-Quiñones, F. R.; Bergamasco, R.; Pereira, N. C. Monolayer-Multilayer Adsorption Phenomenological Model: Kinetics, Equilibrium and Thermodynamics. *Chem. Eng. J.* **2016**, *284*, 1328–1341. https://doi.org/10.1016/j.cej.2015.09.085.

(70) Parhi, P.; Golas, A.; Barnthip, N.; Noh, H.; Vogler, E. A. Volumetric Interpretation of Protein Adsorption: Capacity Scaling with Adsorbate Molecular Weight and Adsorbent Surface Energy. *Biomaterials* **2009**. https://doi.org/10.1016/j.biomaterials.2009.09.005.

(71) Buttersack, C. Modeling of Type IV and v Sigmoidal Adsorption Isotherms. *Phys. Chem. Chem. Phys.* **2019**. https://doi.org/10.1039/c8cp07751g.

(72) Hellner, B.; Lee, S. B.; Subramaniam, A.; Subramanian, V. R.; Baneyx, F. Modeling the Cooperative Adsorption of Solid-Binding Proteins on Silica: Molecular Insights from Surface Plasmon Resonance Measurements. *Langmuir* **2019**.

https://doi.org/10.1021/acs.langmuir.9b00283.

(73) Mudunkotuwa, I. A.; Minshid, A. Al; Grassian, V. H. ATR-FTIR Spectroscopy as a Tool to Probe Surface Adsorption on Nanoparticles at the Liquid–Solid Interface in Environmentally and Biologically Relevant Media. *Analyst* **2014**, *139* (5), 870–881. https://doi.org/10.1039/C3AN01684F.

(74) Thomson, A. J.; Gray, H. B. Bio-Inorganic Chemistry. *Current Opinion in Chemical Biology*. 1998. https://doi.org/10.1016/S1367-5931(98)80056-2.

(75) Surewicz, W. K.; Mantsch, H. H. New Insight into Protein Secondary Structure from Resolution-Enhanced Infrared Spectra. *Biochimica et Biophysica Acta (BBA)/Protein Structure and Molecular* **1988**. https://doi.org/10.1016/0167-4838(88)90107-0.

(76) Jackson, M.; Mantsch, H. H. Artifacts Associated with the Determination of Protein Secondary Structure by ATR-IR Spectroscopy. *Appl. Spectrosc.* **1992**. https://doi.org/10.1366/0003702924124862.

(77) Dockal, M.; Carter, D. C.; Rüker, F. Conformational Transitions of the Three Recombinant Domains of Human Serum Albumin Depending on PH. *J. Biol. Chem.* **2000**. https://doi.org/10.1074/jbc.275.5.3042.

(78) Park, Y. J.; Kim, K. H.; Lim, D. W.; Lee, E. K. Effects of PH and Protein Conformation on In-Solution Complexation between Bovine α-Lactalbumin and Oleic Acid: Binding Trend Analysis by Using SPR and ITC. *Process Biochem.* **2015**. https://doi.org/10.1016/j.procbio.2015.05.018.

(79) Chamani, J.; Moosavi-Movahedi, A. A.; Rajabi, O.; Gharanfoli, M.; Momen-Heravi, M.; Hakimelahi, G. H.; Neamati-Baghsiah, A.; Varasteh, A. R. Cooperative α-Helix Formation of β-Lactoglobulin Induced by Sodium n-Alkyl Sulfates. *J. Colloid Interface Sci.* **2006**, *293* (1), 52–60. https://doi.org/10.1016/j.jcis.2005.06.015.

(80) Kizewski, F. R.; Boyle, P.; Hesterberg, D.; Martin, J. D. Mixed Anion (Phosphate/Oxalate) Bonding to Iron(III) Materials. *J. Am. Chem. Soc.* **2010**. https://doi.org/10.1021/ja908807b.

(81) Fu, Z.; Wu, F.; Song, K.; Lin, Y.; Bai, Y.; Zhu, Y.; Giesy, J. P. Competitive Interaction between Soil-Derived Humic Acid and Phosphate on Goethite. *Appl. Geochemistry* **2013**. https://doi.org/10.1016/j.apgeochem.2013.05.015.

(82) Gerke, J. Phosphate Adsorption by Humic/Fe-Oxide Mixtures Aged at PH 4 and 7 and by Poorly Ordered Fe-Oxide. *Geoderma* **1993**. https://doi.org/10.1016/0016-7061(93)90074-U.